

1 **Ultrathin High-Mobility SWCNT Transistors with Electrodes Printed by Nanoporous
2 Stamp Flexography**

3 Dhanushkodi D. Mariappan¹, Sanha Kim^{1,2}, Junjie Zhao³, Hangbo Zhao¹, Ulrich Muecke¹, Karen
4 Gleason³, Akintunde Ibitayo Akinwande⁴, A. John Hart^{1*}

5 ¹Department of Mechanical Engineering, Massachusetts Institute of Technology, Cambridge, MA 02139,
6 USA.

7 ²Department of Mechanical Engineering, Korea Advanced Institute of Science and Technology, Daejeon
8 34141, South Korea.,

9 ³Department of Chemical Engineering, Massachusetts Institute of Technology, Cambridge, MA 02139, USA.

10 ⁴Department of Electrical Engineering and Computer Science, Massachusetts Institute of Technology,
11 Cambridge, MA 02139, USA.

12

13 *Corresponding author: ajhart@mit.edu

14

15 **Abstract**

16 To achieve high-performance printed electronic devices, scalable and cost-effective printing of high-
17 quality metallic electrodes with narrow gaps, such for transistors with short channel lengths, is desirable.
18 Here, we demonstrate short channel (<10 μ m) transistors, using thin (< 100-200 nm) electrodes fabricated
19 by flexographic printing with nanoporous stamps, with single-wall carbon nanotubes (SWCNTs) as the
20 network semiconductor. The nanoporous stamps comprise polymer-coated vertically aligned carbon
21 nanotubes (CNTs) and facilitate control of the printed ink thickness in the 50-200 nm range. The
22 measured on-off ratio and mobility meet or exceed those of previously reported SWCNT network
23 transistors fabricated by alternative printing methods.

24

25 **Keywords:** printed electrodes, transistors, flexography, nanoporous stamps, SWCNT networks

26

27

1 **Main Text**

2 High-throughput, cost-effective manufacturing of electronics including radio frequency identification
3 (RFID) tags¹, gas sensors, and light emitting diodes (LEDs) is essential to broader availability of
4 technologies such as smart packages, wearable displays, and skin-conforming medical devices²⁻⁶. To
5 expand the use of electronics in such daily-life products, silicon microfabrication processes are limited in
6 terms of cost, throughput and substrate flexibility. Printed electronics utilizing scalable printing
7 technologies, such as inkjet, screen printing, gravure and flexography are promising alternatives.
8 Therefore, a massive number of research, development and production of printed electronic devices has
9 been reported in the last two decades⁷⁻¹⁰.

10 Transistors are a basic building block of printed electronics, and the transistor quality and performance
11 are driven by the choice of materials, degree of miniaturization, and dimensional precision. For example,
12 the performance of the printed displays^{11,12} is driven by the thickness and the switching speed of the
13 constituent thin-film transistors^{13,14}. The speed of a thin-film transistor depends mainly on the
14 semiconductor carrier mobility and the channel length, measured by the distance between the source and
15 drain electrodes. Thick and non-uniform dielectric and electrode layers in transistors lead to lower
16 breakdown voltages due to large localized electric fields¹³. Therefore, the performance of transistors
17 manufactured by printing technologies are correlated with lateral resolution and minimum thickness of
18 extant methods⁹.

19 Most of printing technologies for electronics use liquid or polymeric inks, often containing colloidal
20 nanoparticles that are annealed to form films after evaporation of the carrier solvent. As such, limitations
21 to the feature size and thickness are attributed to the coupled, time-dependent fluid and solid mechanics of
22 the printing process. Recently, flexographic printing with significantly finer printed feature dimensions
23 was achieved using nanoporous stamps instead of traditional non-porous polymer stamps.⁹ The
24 nanoporous stamps can retain the ink within their volume^{9,15}, enabling the printed pattern to precisely
25 replicate the shape of stamp features without suffering the squeeze-out and dewetting instabilities that are
26 common in traditional flexography with non-porous elastomeric stamps. Nanoporous flexography, which
27 is capable of printing conductive, dielectric, and semiconducting nanoparticle inks into features having ~3
28 μm minimum width and ~30-50 nm thickness at high speed (0.1 m/s)^{9,16}, is therefore attractive for
29 printing high performance transistors as elements of future integrated devices.

30 Here, we demonstrate thin (< 100-500 nm), short channel (<10 μm) transistors, using electrodes fabricated
31 by flexographic printing with nanoporous stamps, with single-wall carbon nanotubes (SWCNTs) as the
32 network semiconductor. We designed and fabricated a bottom gate, top-contact transistor as shown in
33 [Fig.1A](#). The device consists of a p-doped silicon gate electrode (resistance = 0.001-0.005 $\Omega\text{-cm}$, thickness
34 = 500 μm), thermally grown silicon dioxide (thickness = 300 nm, University Wafer Product No. 1583)
35 dielectric layer, silver source and drain electrodes (thickness ~100-200 nm), and SWCNT network
36 semiconducting layer.

37 Flexographic printing of silver electrodes was achieved with nanoporous stamps comprising vertically
38 aligned carbon nanotubes (CNTs) which are conformally coated with polymer via initiated chemical
39 vapor deposition (iCVD, [Fig.1B](#)). We inked the stamp via spin-coating, and the high porosity (~90%) of
40 the prepared stamp allows to retain the liquid ink within their volume. Using the inked stamp designed
41 according to the device, the source and drain electrode pattern ([Fig. 1C](#)) was printed directly onto the
42 oxide-coated silicon wafer. For successful printing, control of contact pressure was essential, and must lie

1 within a range determined by the stiffness of the CNTs, CNT-CNT spacing, and the standard deviation of
2 the lengths of CNTs.^{9,15} In a prior work, we estimate the pressure range where the area ratio (ratio of area
3 of stamp pattern to printed pattern) is ~ 1 using experiments and analytical modeling. The thickness of the
4 printed layer can be controlled via the speed at which the stamp is retracted away from the substrate after
5 contact. During printing, in a custom-built plate-to-plate printing apparatus⁹, we brought the stamp into
6 contact with the wafer and apply a contact pressure of ~50 to 100 kPa using a weight. After maintaining
7 contact for ~15 s, we retracted the stamp quasi-statically (~1 mm/s) enabling printing of layers with
8 thickness > 200nm after solvent evaporation.

9 The liquid ink (736511, Sigma Aldrich) contained <10 nm silver nanoparticles dispersed in tetradecane
10 with ~50-60% weight concentration. After drying for 2 mins in ambient conditions, the substrate with the
11 printed ink pattern was annealed to retain the electrical conductivity by sintering the metal particles into a
12 continuous film (Fig. 2A-C). Here, the annealing condition needs to be appropriately controlled
13 considering the printed thickness, as excessive temperature and/or annealing time can cause dewetting
14 and breakup of the Ag film. Annealing was performed in ambient conditions on a hot plate with a set
15 temperature of 200-500 °C¹⁷. Higher annealing temperature and longer annealing time results in greater
16 grain size therefore can enhance the electrical conductivity, yet voids may form once the local metal grain
17 size exceed the layer thickness and therefore the conductivity reduces. At sintering temperatures below
18 300 °C coarsening and densification is insufficient and at temperatures above 300 °C, though continuous
19 films with large grains form locally, several voids form and this can lead to large variations in the
20 measured conductivity of the sintered films (Fig. 2D). At sintering temperature of 300 °C, it is possible to
21 form continuous layers with few voids for printed layers of thicknesses varying from 50 to 250 nm (Fig.
22 2E). With appropriate annealing, the measured conductivity (Fig. 2F, 2G) of the annealed source and
23 drain electrodes was 4.25×10^7 S/m, which is 70% of that of bulk silver.

24 The annealing condition should be adjusted according to the printing thickness. For experimental
25 investigation, we printed electrodes with different thickness of ~50 nm, 110 nm, and 185 nm (Fig. 2C).
26 We observed the SEM images of the annealed samples to assess the continuity of films qualitatively (Fig.
27 2E). For the thinnest layers (~50nm), dewetting leads to discontinuities in the sintered layers. The
28 resistance of the sintered layers was measured by printing lines of length ~850 μm and width ~10 μm
29 (Fig. 2G). The resistance decreases with increasing sintering temperature for lines of thicknesses >100nm.
30 (Fig. 2G). At 250 °C sintering temperature, resistance is high and has the largest variation with thickness.
31 At 350 °C sintering temperature, resistance is the lowest for all thicknesses but there is large variation
32 with thickness. But, at 300 °C sintering temperature, for printed films of t_{av} ~50- 250nm, resistance has
33 minimum variation with thickness. Therefore, 300 °C was determined to be the optimal sintering
34 temperature, and good quality features with conductivity of 4.4×10^7 S/m (~70% of bulk silver) and the
35 minimum sintering time is ~ 1 min.

36 We selected SWCNTs as the semiconducting layer, owing to the compatibility of solution-based SWCNT
37 deposition with non-lithographic fabrication. The performance of CNT network transistors strongly
38 depends not only on the quality of individual CNTs but also the CNT density. We deposited the
39 semiconducting layer on top of our printed S/D electrodes via spincoating, and the density was tunable by
40 the droplet volume, spincoating speed and duration. Here, a 300 μl droplet of ink (NanoIntegris, IsoSol-
41 S100, 99.9% purity) was pipetted onto the wafer and then the wafer was spun to 1500 rpm for 15 seconds
42 in a spincoater (Specialty Coating Systems, G3P SPINCOAT). No surface pretreatment was used before
43 deposition. The measured density of the network of SWNCTs is ~100 SWCNTs/μm² (Fig. 3A, Fig.S1)
44 which is above the percolation threshold^{18,19} (> 40 SWCNTs/μm²) resulting in high on-conductance and
45 mobility.

1 The transfer characteristics of the fabricated transistors were measured by varying V_g from -10V to +10V
2 and measuring I_d for $V_d = 1V, 5V, 7V, 9V, 10V$. [Fig. 3B](#), [Fig. S2](#) shows the transfer characteristics for the
3 transistor with a channel length of 7 μm . The on-off ratio of the transistors exceeded 10^3 and the threshold
4 voltage varied from 1 V to 8 V. The mobility is calculated based on the slope of the plot of $\sqrt{I_d}$ against
5 V_g using the following equation (see Supporting Information)

6

$$\sqrt{I_d} = \sqrt{\frac{\mu C_{ox} W}{2L}} (V_g - V_T)$$

7 where μ , C_{ox} , and V_T are the mobility, oxide capacitance and threshold voltage respectively. [Fig. S3](#)
8 compares the transfer characteristics at $V_d = 1V$ for three transistors with channel lengths of 6.6, 12.4, and
9 146 μm . The mobility increases from $13.8 \text{ cm}^2/\text{Vs}$ for $L = 12.4 \mu m$ to $39.5 \text{ cm}^2/\text{Vs}$ for $L = 146 \mu m$ ([Table S1](#)). The mobility variation with channel length is likely due to the variation in the SWCNT network
10 density between the devices of different channel lengths. The extracted mobility is also likely affected by
11 the contact resistance and its variations. The low on-off ratio is likely due to high contact resistance. The
12 output resistance calculated from the output characteristics ([Fig. S4](#)) does not vary significantly with the
13 gate voltage, which is one of the indicators of high contact resistance in the device.

14 The on-off ratio and the mobility of our transistors were determined in the range of 10^3 - 10^4 and ~ 13 - 39 ,
15 respectively, which are comparable to other printed transistors ([Fig. 3C and 3D](#)).^{7,8,20-27} The total thickness
16 of the device excluding the gate (p-doped Si) layer is ~ 400 - 600 nm which is thinner than other printed
17 transistors reported in literature.^{13,28} With nanoporous stamps, ultra-thin layers can be printed as the ink
18 transfer volume per unit length is the lowest as compared to other printing processes⁹. Notably, nanoporous
19 stamps can be adopted to continuous manufacturing by fabricating CNTs on a roller and using a continuous
20 inking system. In prior work, we have shown also compatibility with continuous printing in a plate to roll
21 format, and the combination of speed (>200 mm/s) and resolution ($\sim 3 \mu m$) surpasses published process
22 capabilities for flexography, gravure, inkjet and screen printing processes⁹.

23 We have demonstrated a TFT with good performance characteristics. To demonstrate a fully printed
24 device on flexible substrates, printing of gate and dielectrics and optimization of sintering conditions are
25 required and we expect these can be achieved. The printing of SWCNT networks can also be studied. By
26 using layer to layer registration and achieving a designed overlap between the S/D electrodes and
27 dielectric layer, leakage currents can be reduced to achieve even higher on-off ratios ($>10^4$) than what has
28 been achieved in this work.

29
30

1 **Supporting Information**

2 Fabrication of transistor by printing silver nanoparticles and forming a continuous layer by sintering and
3 deposition of SWCNT networks with organic solvent based ink, Transfer characteristics of the transistor
4 (channel length 7 μm) for drain voltages varying from 1-10V, Transfer Characteristics of the transistors
5 with channel lengths varying from 6.6 to 146 μm plotted as $\sqrt{I_d}$ against V_g for calculation of mobility and
6 on-off ratio, Output characteristics of the transistor (channel length 7 μm) for gate voltages varying from -
7 3V to -0.5V, On-off ratio and mobility values for the transistors calculated from the transfer characteristics,
8 Mobility calculation using model for linear region.

9

10 **Acknowledgements**

11 Financial support was provided by the National Science Foundation (CMMI-1463344, CMMI-1826216),
12 the MIT Energy Initiative Seed Fund, the MIT-Skoltech Next Generation Program (First Round, 2016-
13 2019), and BAE Systems. We thank Ahmad Zubair, Elaine McVay, and Marek Hempel for assistance in
14 measurements of transfer characteristics. CNT catalyst deposition and patterning were performed at the
15 MIT Microsystems Technology Laboratory (MTL). Electron microscopy and profilometry were performed
16 at the shared experimental facilities at the MIT Center for Materials Science and Engineering (CMSE)
17 supported in part by the MRSEC Program of the National Science Foundation under award number DMR-
18 1419807.

19

20 **Methods**

21 **Stamp Fabrication** The stamp consists of source and drain electrodes with different channel lengths ($L=5$ -
22 $150\mu\text{m}$) and fixed width ($W=200\mu\text{m}$). An exemplary stamp is shown in [Fig. 1B](#). To fabricate the stamps⁹,
23 first vertically aligned CNT arrays (CNT ‘forests’) are grown on lithographically patterned silicon
24 substrates by atmospheric pressure chemical vapor deposition (CVD). Then, the top entangled ‘crust’ layer
25 ($<1\mu\text{m}$ thickness) is removed by a brief oxygen plasma etching (Diener, Femto Plasma System) and coated
26 with a thin layer ($\sim 20\text{ nm}$) of poly-perfluorodecylacrylate (pPFDA) using initiated CVD (iCVD).^{9,29,30} The
27 plasma etching is critical to remove the stiff and rough crust which is not desirable for high-resolution
28 printing because it results in non-uniform contact against the target substrate. The pPFDA coating followed
29 by second plasma treatment allow liquid infiltration and solvent evaporation without shrinkage or collapse
30 of the CNT forest by elastocapillary densification. The final plasma-treated pPFDA-CNT microstructures
31 are highly porous ($>90\%$ porosity) with nanometer pore size ($\sim 100-200\text{ nm}$), allow liquid infiltration
32 without deformation due to capillary forces, and are mechanically compliant, enabling uniform contact with
33 the target substrates.

34 **Inking** The ink used in this study is composed of silver nanoparticles dispersed in tetradecane (Sigma-
35 Aldrich, 736511). The surface tension and viscosity of the ink are 27 mN/m and 10 mPa-s, respectively,
36 and the ink exhibits good conductivity (30-60% of bulk silver) after annealing.⁹ The particle concentration
37 is 50-60 wt% with particle sizes less than 10 nm. A 100 μl droplet of ink is pipetted onto the stamp and
38 then the stamp is spun to 1500 rpm for 1-3 minutes in a spincoater.

1 **Annealing** A hot plate was used to do rapid annealing of the silver nanoparticles after printing the silver
2 ink. The hot plate was set to the 300 °C and the stamps were placed on the hotplate after it reached the
3 setpoint. The stamps were left on the hot plate for 1 minute for annealing.

4 **Device Characterization** A DC probe station and semiconductor parameter analyzer (Agilent 4155C,
5 Easy Expert software) were used for the measurement of conductivity of the annealed electrodes, and the
6 transfer characteristics of the TFTs.

7

8

1 **References**

2 (1) Want, R. A Key to Automating Everything Already Common in Security Systems. *Sci Am*
3 **2004**, *290* (1), 56–65.

4 (2) Vena, A.; Perret, E.; Tedjini, S.; Tourtollet, G. E. P.; Delattre, A.; Garet, F.; Boutant, Y.
5 Design of Chipless RFID Tags Printed on Paper by Flexography. *IEEE Trans Antennas
6 Propag* **2013**, *61* (12), 5868–5877. <https://doi.org/10.1109/TAP.2013.2281742>.

7 (3) Ostfeld, A. E.; Deckman, I.; Gaikwad, A. M.; Lochner, C. M.; Arias, A. C. Screen Printed
8 Passive Components for Flexible Power Electronics. *Sci Rep* **2015**, *5*, 1–11.
9 <https://doi.org/10.1038/srep15959>.

10 (4) Wang, X.; Zhang, Y.; Guo, R.; Wang, H.; Yuan, B.; Liu, J. Conformable Liquid Metal
11 Printed Epidermal Electronics for Smart Physiological Monitoring and Simulation
12 Treatment. *Journal of Micromechanics and Microengineering*. Institute of Physics
13 Publishing February 5, 2018. <https://doi.org/10.1088/1361-6439/aaa80f>.

14 (5) Kuberský, P.; Syrový, T.; Hamacek, A.; Nešpůrek, S.; Stejskal, J. Printed Flexible Gas
15 Sensors Based on Organic Materials. In *Procedia Engineering*; Elsevier Ltd, 2015; Vol.
16 120, pp 614–617. <https://doi.org/10.1016/j.proeng.2015.08.746>.

17 (6) Gao, W.; Ota, H.; Kiriya, D.; Takei, K.; Javey, A. Flexible Electronics toward Wearable
18 Sensing. *Acc Chem Res* **2019**, *52* (3), 523–533.
19 <https://doi.org/10.1021/acs.accounts.8b00500>.

20 (7) Grubb, P. M.; Mokhtari Koushyar, F.; Lenz, T.; Asghari, A.; Gan, G.; Xia, W.; Dalir, H.;
21 Subbaraman, H.; Chen, R. T. High Speed Roll-to-Roll Printable Transistor Enabled by a
22 Pulsed Light Curable CNT Ink. *Journal of Manufacturing and Materials Processing* **2019**,
23 *3* (2), 33. <https://doi.org/10.3390/jmmp3020033>.

24 (8) Lau, P. H.; Takei, K.; Wang, C.; Ju, Y.; Kim, J.; Yu, Z.; Takahashi, T.; Cho, G.; Javey, A.
25 Fully Printed, High Performance Carbon Nanotube Thin-Film Transistors on Flexible
26 Substrates. **2013**. <https://doi.org/10.1021/nl401934a>.

27 (9) Kim, S.; Sojoudi, H.; Zhao, H.; Mariappan, D.; McKinley, G. H.; Gleason, K. K.; Hart, A.
28 J. Ultrathin High-Resolution Flexographic Printing Using Nanoporous Stamps. *Sci Adv*
29 **2016**, *2* (12), e1601660. <https://doi.org/10.1126/sciadv.1601660>.

30 (10) Reddy, A. S. G.; Narakathu, B. B.; Eshkeiti, A.; Bazuin, B. J.; Joyce, M.; Atashbar, M. Z.
31 Fully Printed Organic Thin Film Transistors (OTFT) Based Flexible Humidity Sensors. In
32 *Proceedings of IEEE Sensors*; IEEE Computer Society, 2013.
33 <https://doi.org/10.1109/ICSENS.2013.6688309>.

34 (11) Wang, C.; Zhang, J.; Ryu, K.; Badmaev, A.; Arco, L. G. De; Zhou, C. Wafer-Scale
35 Fabrication of Separated Carbon Nanotube Thin-Film Transistors for Display Applications.
36 **2009**. <https://doi.org/10.1021/nl902522f>.

37 (12) Suzuki, K.; Yutani, K.; Nakashima, M.; Onodera, A.; Mizukami, S.; Kato, M.; Tano, T.;
38 Tomono, H.; Yanagisawa, M.; Kameyama, K. All-Printed Organic TFT Backplanes for
39 Flexible Electronic Paper. **2010**, 1–6.

1 (13) Fukuda, K.; Someya, T. Recent Progress in the Development of Printed Thin-Film
2 Transistors and Circuits with High-Resolution Printing Technology. *Advanced Materials*
3 **2017**, *29* (25). <https://doi.org/10.1002/adma.201602736>.

4 (14) Khan, S.; Lorenzelli, L.; Dahiya, R. S. Technologies for Printing Sensors and Electronics
5 over Large Flexible Substrates: A Review. *IEEE Sens J* **2015**, *15* (6), 3164–3185.
6 <https://doi.org/10.1109/JSEN.2014.2375203>.

7 (15) Mariappan, D. D.; Kim, S.; Boutilier, M. S. H.; Zhao, J.; Zhao, H.; Beroz, J.; Muecke, U.;
8 Sojoudi, H.; Gleason, K.; Brun, P. T.; Hart, A. J. Dynamics of Liquid Transfer from
9 Nanoporous Stamps in High-Resolution Flexographic Printing. *Langmuir* **2019**, *35* (24),
10 7659–7671. <https://doi.org/10.1021/acs.langmuir.9b00460>.

11 (16) Mariappan, D. D.; Kim, S.; Hart, A. J. A Precision Desktop Plate-to-Roll Apparatus for
12 Development of Advanced Flexographic Printing Processes. *Precis Eng* **2020**, *66*
13 (January), 392–400. <https://doi.org/10.1016/j.precisioneng.2020.07.012>.

14 (17) Kim, J.; Oh, J.; Jung, K.-M.; Park, K.; Kim, Y.-S.; Jeon, J.-H. Ultrathin Flexible Thin Film
15 Transistors with CYTOP Encapsulation by Debonding Process. *Semicond Sci Technol*
16 **2019**. <https://doi.org/10.1088/1361-6641/ab2201>.

17 (18) Kocabas, C.; Pimparkar, N.; Yesilyurt, O.; Kang, S. J.; Alam, M. A.; Rogers, J. A.
18 Experimental and Theoretical Studies of Transport through Large Scale, Partially Aligned
19 Arrays of Single-Walled Carbon Nanotubes in Thin Film Type Transistors. *Nano Lett*
20 **2007**, *7* (5), 1195–1202. <https://doi.org/10.1021/nl062907m>.

21 (19) Zhou, Y.; Gaur, A.; Hur, S.-H.; Kocabas, C.; Meitl, M. a; Shim, M.; Rogers, J. a. P-
22 Channel, n-Channel Thin Film Transistors and P–n Diodes Based on Single Wall Carbon
23 Nanotube Networks. *Nano Lett* **2004**, *4* (10), 2031–2035.
24 <https://doi.org/10.1021/nl048905o>.

25 (20) Yu, M.; Wan, H.; Cai, L.; Miao, J.; Zhang, S.; Wang, C. Fully Printed Flexible Dual-Gate
26 Carbon Nanotube Thin-Film Transistors with Tunable Ambipolar Characteristics for
27 Complementary Logic Circuits. *ACS Nano* **2018**, *12* (11), 11572–11578.
28 <https://doi.org/10.1021/acsnano.8b06748>.

29 (21) Cao, C.; Andrews, J. B.; Kumar, A.; Franklin, A. D. Improving Contact Interfaces in Fully
30 Printed Carbon Nanotube Thin-Film Transistors. *ACS Nano* **2016**, *10* (5), 5221–5229.
31 <https://doi.org/10.1021/acsnano.6b00877>.

32 (22) Homenick, C. M.; James, R.; Lopinski, G. P.; Dunford, J.; Sun, J.; Park, H.; Jung, Y.; Cho,
33 G.; Malenfant, P. R. L. Fully Printed and Encapsulated SWCNT-Based Thin Film
34 Transistors via a Combination of R2R Gravure and Inkjet Printing. *ACS Appl Mater
35 Interfaces* **2016**, *8* (41), 27900–27910. <https://doi.org/10.1021/acsami.6b06838>.

36 (23) Schießl, S. P.; Fröhlich, N.; Held, M.; Gannott, F.; Schweiger, M.; Forster, M.; Scherf, U.;
37 Zaumseil, J. Polymer-Sorted Semiconducting Carbon Nanotube Networks for High-
38 Performance Ambipolar Field-Effect Transistors. *ACS Appl Mater Interfaces* **2015**, *7* (1),
39 682–689. <https://doi.org/10.1021/am506971b>.

1 (24) Miyata, Y.; Shiozawa, K.; Asada, Y.; Ohno, Y.; Kitaura, R.; Mizutani, T.; Shinohara, H.
2 Length-Sorted Semiconducting Carbon Nanotubes for High-Mobility Thin Film
3 Transistors. *Nano Res* **2011**, *4* (10), 963–970. <https://doi.org/10.1007/s12274-011-0152-7>.

4 (25) Cao, C.; Andrews, J. B.; Franklin, A. D. Completely Printed, Flexible, Stable, and
5 Hysteresis-Free Carbon Nanotube Thin-Film Transistors via Aerosol Jet Printing. *Adv
6 Electron Mater* **2017**, *3* (5), 1–10. <https://doi.org/10.1002/aelm.201700057>.

7 (26) Lee, H. W.; Yoon, Y.; Park, S.; Oh, J. H.; Hong, S.; Liyanage, L. S.; Wang, H.; Morishita,
8 S.; Patil, N.; Park, Y. J.; Park, J. J.; Spakowitz, A.; Galli, G.; Gygi, F.; Wong, P. H. S.;
9 Tok, J. B. H.; Kim, J. M.; Bao, Z. Selective Dispersion of High Purity Semiconducting
10 Single-Walled Carbon Nanotubes with Regioregular Poly(3-Alkylthiophene)s. *Nat
11 Commun* **2011**, *2* (1). <https://doi.org/10.1038/ncomms1545>.

12 (27) Molina-Lopez, F.; Gao, T. Z.; Kraft, U.; Zhu, C.; Öhlund, T.; Pfattner, R.; Feig, V. R.;
13 Kim, Y.; Wang, S.; Yun, Y.; Bao, Z. Inkjet-Printed Stretchable and Low Voltage Synaptic
14 Transistor Array. *Nat Commun* **2019**, *10* (1). <https://doi.org/10.1038/s41467-019-10569-3>.

15 (28) White, M. S.; Kaltenbrunner, M.; Głowacki, E. D.; Gutnichenko, K.; Kettlgruber, G.; Graz,
16 I.; Aazou, S.; Ulbricht, C.; Egbe, D. A. M.; Miron, M. C.; Major, Z.; Scharber, M. C.;
17 Sekitani, T.; Someya, T.; Bauer, S.; Sariciftci, N. S. Ultrathin, Highly Flexible and
18 Stretchable PLEDs. *Nat Photonics* **2013**, *7* (10), 811–816.
19 <https://doi.org/10.1038/nphoton.2013.188>.

20 (29) Gupta, M.; Gleason, K. K. Initiated Chemical Vapor Deposition of Poly(1H,1H,2H,2H-
21 Perfluorodecyl Acrylate) Thin Films. *Langmuir* **2006**, *22* (24), 10047–10052.
22 <https://doi.org/10.1021/la061904m>.

23 (30) Sojoudi, H.; Kim, S.; Zhao, H.; Annavarapu, R. K.; Mariappan, D.; Hart, A. J.; McKinley,
24 G. H.; Gleason, K. K. Stable Wettability Control of Nanoporous Microstructures by ICVD
25 Coating of Carbon Nanotubes. *ACS Appl Mater Interfaces* **2017**, *9* (49).
26 <https://doi.org/10.1021/acsami.7b13713>.

27

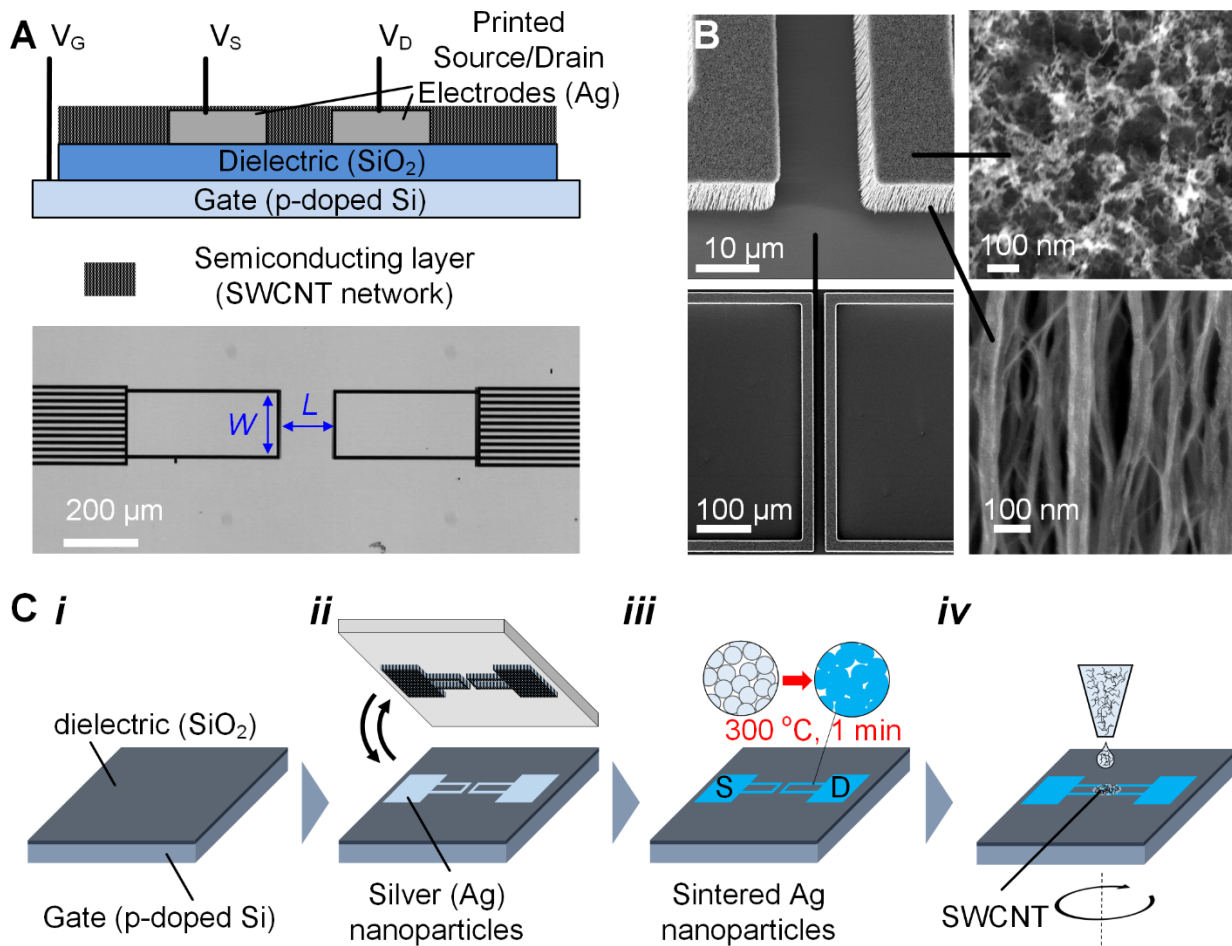


Figure 1. SWCNT transistors with electrodes printed using nanoporous stamps. A) Schematic of the device and top-view microscope image of the CNT-based printing stamp showing the channel geometry defined by the source and drain electrodes. B) SEM images of the stamp, showing the top and sidewall surfaces; channel has 10 μm length, defined by gap between stamp islands. C) Device fabrication steps showing i) p-doped silicon gate electrode with thermally grown silicon dioxide ii) printing of Ag nanoparticle ink to define source and drain electrodes, followed by iii) annealing to sinter the nanoparticles, and then iv) deposition of the semiconducting CNT solution which forms a thin film by spin-coating.

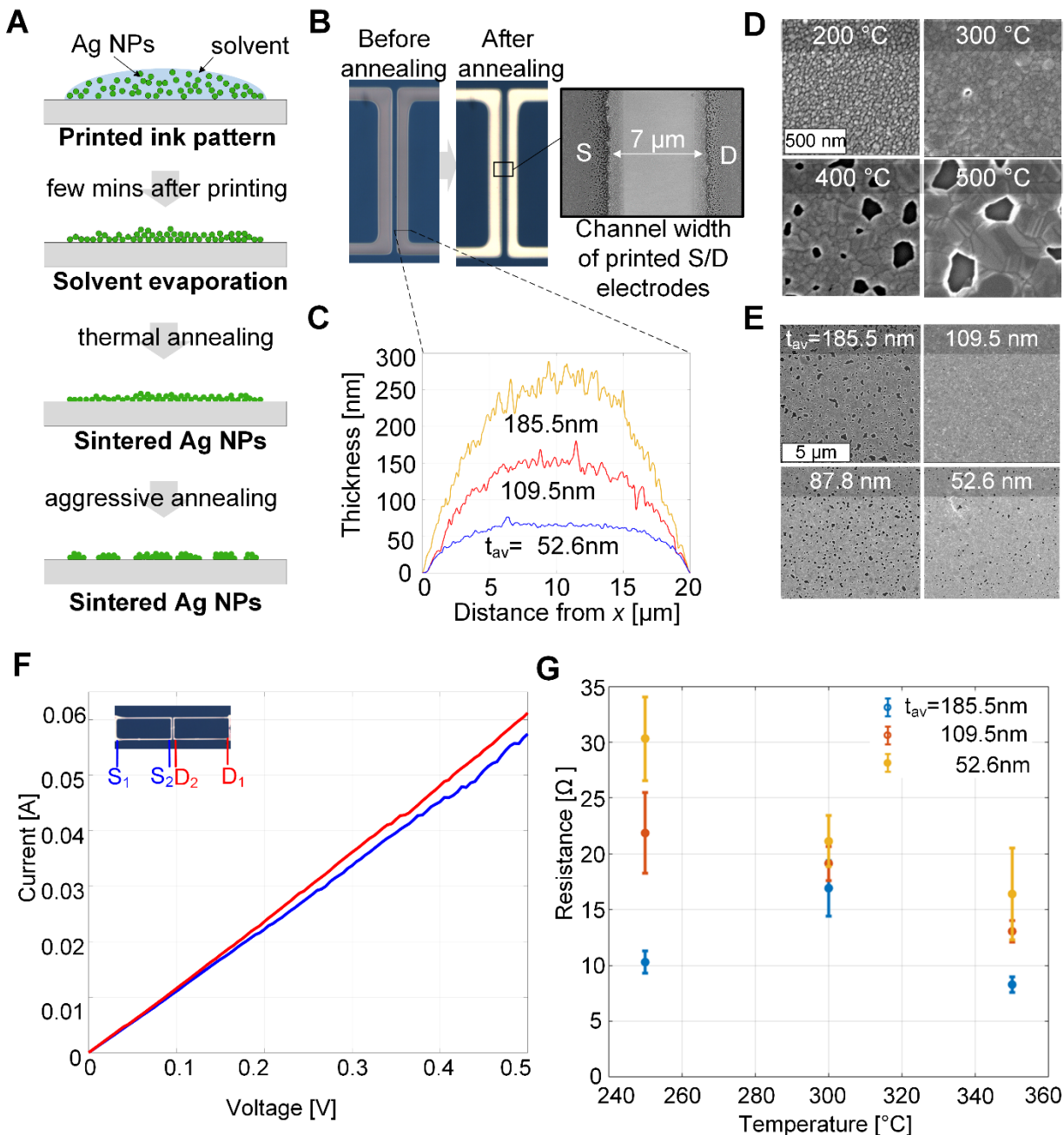


Figure 2. Analysis of sintering of printed Ag nanoparticle inks to conductive electrodes. (A) Schematic of transformation of thin ink film to continuous conductive layer after solvent evaporation and sintering. (B) Optical microscope and SEM images of printed source and drain electrodes. (C) Cross-sectional profiles of printed Ag ink lines before annealing having thicknesses 185.5 nm, 109.5 nm, and 52.6 nm. (D) Comparison of Ag film morphology after annealing at 200, 300, 400, 500 °C for 10 minutes. (E) Comparison of Ag film morphology after annealing at 300 °C for 10 minutes, for corresponding as-printed ink thicknesses. (F) IV characteristics of the source and drain electrodes exhibiting conductivity of ~70% of bulk silver after appropriate annealing. (G) Resistance of printed electrodes according to printed layer thickness and annealing temperature (times fixed to 10 minutes).

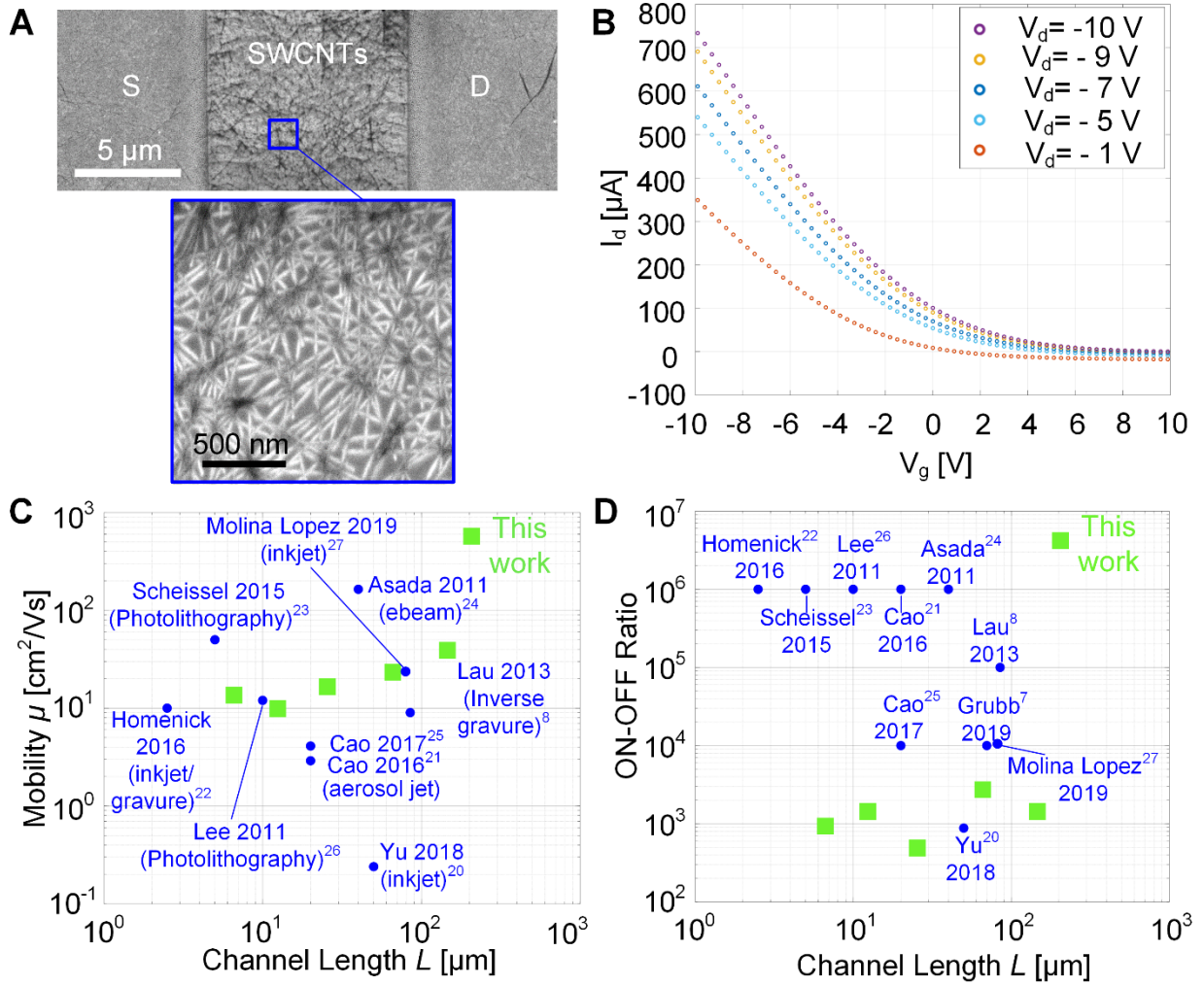


Figure 3. Characteristics of SWCNT transistors fabricated using sintered Ag electrodes.
 (A) SEM images of spincoated SWCNT film on top of Ag electrodes. (B) transfer characteristics of the transistor (channel length 7 μm) for drain voltages varying from -10V to -1V. (C) Mobility and (D) on-off ratio according to the channel length of the transistors reported in this work, and comparison with other previous SWCNT-based transistors.